Available online at www.sciencedirect.com

ScienceDirect

Publishing Services by Elsevier

International Journal of Naval Architecture and Ocean Engineering 8 (2016) 475–486

http://www.journals.elsevier.com/international-journal-of-naval-architecture-and-ocean-engineering/

Optimal design of hydraulic support landing platform for a four-rotor dish-shaped UUV using particle swarm optimization

Bao-Shou Zhang*, Bao-Wei Song, Jun Jiang, Zhao-Yong Mao

School of Marine Science and Technology, Northwestern Polytechnical University, Shaanxi, China

Received 24 January 2016; revised 23 May 2016; accepted 30 May 2016
Available online 15 July 2016

Abstract

Four-rotor dish-shaped unmanned underwater vehicles (FRDS UUVs) are new type underwater vehicles. The main goal of this paper is to develop a quick method to optimize the design of hydraulic support landing platform for the new UUV. In this paper, the geometry configuration and instability type of the platform are defined. Computational investigations are carried out to study the hydrodynamic performance of the landing platform using the Computational Fluid Dynamics (CFD) method. Then, the response surface model of the optimization objective is established. The intelligent particle swarm optimization (PSO) is applied to finding the optimal solution. The result demonstrates that the stability of landing platform is significantly improved with the global objective index increasing from 1.045 to 1.158 (10.86% higher) after the optimization process.

Keywords: Four-rotor dish-shaped UUV; Hydraulic support; Particle swarm optimization; Response surface model; Computational fluid dynamics

1. Introduction

The wide application of Unmanned Underwater Vehicles (UUVs) affects tremendously the development of the ocean exploration. Long time reconnaissance and exploration at a certain area on the seabed have become an imperative task. So the ability of landing or mooring on the seabed is necessary for these UUVs. The application of landing on the seabed has stepped up the demands upon the optimal design of landing or mooring platform for UUVs. In recently, the research of landing or mooring mode for a UUV has become an international hot issue.

There are two main types of landing or mooring mode: mooring platform and bottom resting platform using hydraulic support. As for mooring platform, numerical differential models between mooring chain and seabed had been studied and improved for a floating platform (Huston and Kamman, 1982; Wang et al., 2010). Similarly, a finite difference method for of mooring chains had been analyzed for an underwater flight vehicle (Feng and Allen, 2004). Then, the influence of external disturbance factors on mooring system was taken into account (Cerveira et al., 2013). The landing platforms have the advantage of simple structure, but they are more easily affected by ocean currents and it is difficult for them to keep at a stable attitude. Hydrodynamic characteristics and stability of UUV parking on the seabed have been analyzed for bottom resting platform (Song et al., 2012). Disturbance factors from the seabed are stumbling block for the performance of the landing platform. So the hydraulic support is incorporated into the landing system. The advantages of bottom resting platform with hydraulic supports, such as move away from the distractions of the seabed and extended-duration deployments, rely on the shape and layout which has excellent high stability.

In this paper, the FRDS UUV is a new unmanned underwater vehicle designed in Northwestern Polytechnical

* Corresponding author.
E-mail address: 1262034751@qq.com (B.-S. Zhang).
Peer review under responsibility of Society of Naval Architects of Korea.

http://dx.doi.org/10.1016/j.ijnaoe.2016.05.007

University China (Song et al., 2016). The UUV is designed to investigate and explore a certain area on the seabed. Computational Fluid Dynamics (CFD) uses numerical analysis and algorithms to solve and analyze problems that involve fluid flows. Hydrodynamic characteristics of the landing platform were analyzed by using CFD software.

The optimal layout design of the hydraulic support will make the platform staying away from distractions. In engineering, Multi-Objective Programming (MOP) is proposed to found the best comprehensive performances (Liang et al., 2012) for particle swarm optimization. MOP is concerned with mathematical optimization problems involving more than one objective function to be optimized simultaneously. In order to obtain the objective function, correct Design of Experiments (DOE) is important.

Then it is necessary to choose a highly effective optimization method. Many optimization problems from the industrial engineering world are very complex and quite hard to solve by conventional optimization techniques. Inspired by observing the natural swarming behavior of bird flocking, Particle Swarm Optimization (PSO) was proposed (Eberhart and Kennedy, 1995). PSO algorithm is simple in concept, easy to implement and computationally inexpensive, so it attracts the attention of many scholars and researchers. Genetic Algorithm (GA) and PSO have been compared (Juang, 2004), which proved PSO is more simple and effective. PSO has been successfully applied to a wide range of application areas. PSO have been improved for different applications (Angeline, 1998; Andrews, 2006; Chen, 2015). PSO has been applied extensively in electromagnetics optimization (Jin and Rahmat-Samii, 2010), vehicle routing problem (Hu and Wu, 2010) and screening and classification in engineering applications (Chan et al., 2013; Agrawal and Bawane, 2015) etc. However, intelligent and efficient PSO has been little used in ocean engineering from being born.

In this paper, a new procedure for the optimal design of the FRDS UUV landing platform was presented, in which a complete design sequence was established. Hydrodynamic performance of the landing platform was analyzed by Ansys CFX. Multi-objective optimization model was built by response surface analysis. The global objective function was obtained according to the weight of subs. PSO algorithm was used to obtain the optimal solution. Finally, the optimal design scheme was accurately found in the feasible scheme. In conclusion, the comprehensive performances of landing platform are excellent compared with other design schemes.

2. Geometry configuration

The overall appearance of the FRDS UUV is a spheroid which is generated by revolving an ellipse about its short axis. Four propellers, which are uniformly installed on the ducts of the shell, work together as the vectored thrust unit. The manufacture and trial voyage of the FRDS UUV have been finished. Fig. 1(a) shows the four-rotor dish-shaped UUV we produced and Fig. 1(b) shows the schematic of the hydraulic support landing platform of the UUV.

Compared with the traditional underwater vehicle with slender body of revolution, the FRDS UUV has the advantages of high static stability and large bearing capacity. Due to a circular disc appearance, omnidirectional attitude motion is achieved, so the UUV is suitable for a small and complex water environment.

The hydraulic supports are designed and used to build the landing platform of the UUV. They have evident advantages to keep the stability of the FRDS UUV and avoid the interference of the uncertain factors from the seabed. Fig. 2 shows the external and internal structure view of the landing platform.

Several factors, including the shape of UUV, the hydraulic support types, fender positions, the seabed pattern and environmental conditions, should be taken into consideration in the design of a landing platform. In order to determine the system of landing platform, several main parameters are defined and listed in Table 1.

In order to optimize the design, i.e. the landing platform that lead to the minimum responses of the disturbance from ocean currents, the appearance and layout of hydraulic support should be taken into account primarily.

Based on the concept design of the hydraulic support landing platform, empirical design was completed to reduce the overturn moment as an initial design scheme. In this paper, 30 sample points (design schemes) were selected. The hydrodynamic characteristics of the landing platform were got using Ansys CFX, and the response values were obtained. Based on the important degree, the objective weights were obtained using score from experts. Then the global response surface model is established. Finally, PSO algorithm is applied to complete the optimization process. The design procedure schematic is shown in Fig. 3.

2.1. Instability type

Force analysis of landing platform is completed, as shown in Fig. 4. Instability type of the FRDS UUV landing platform is determined in this section. The equilibrium equation of the critical state is established for the two kinds of instability type.

The first kind of instability type: Side slip. When the hydrodynamic drag of the FRDS UUV and hydraulic support in the horizontal exceeds the friction between the fender and seabed, sideslip occurs. The mathematical model for the critical state can be obtained:

$$F_x + F_L - k_0 \cdot \left(G - F_y - N\right) \geq 0 \tag{1}$$

$$F_x = \int_{\Omega_t} [-p\cos(n,x) + \tau\cos(t,x)]d\Omega_t = C_x \frac{1}{2}\rho v_\infty^2 S \tag{2}$$

where F_L is the hydrodynamic drag of hydraulic support; F_x is hydrodynamic drag of the FRDS UUV; C_x is drag coefficient. Hydrodynamic drag and drag coefficient have a relationship as shown in Eq. (2); similarly, F_y is hydrodynamic lift of landing platform, and hydrodynamic forces and coefficients can be gained using Ansys CFX; k_0 represents friction coefficient.

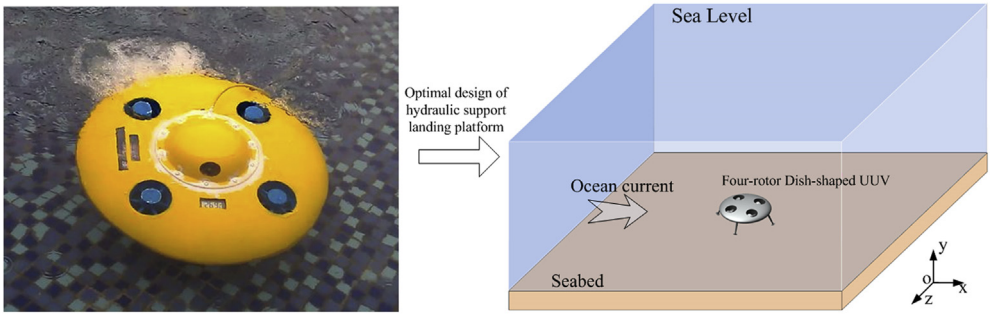

Fig. 1. (a) The FRDS UUV and (b) schematic of the landing platform.

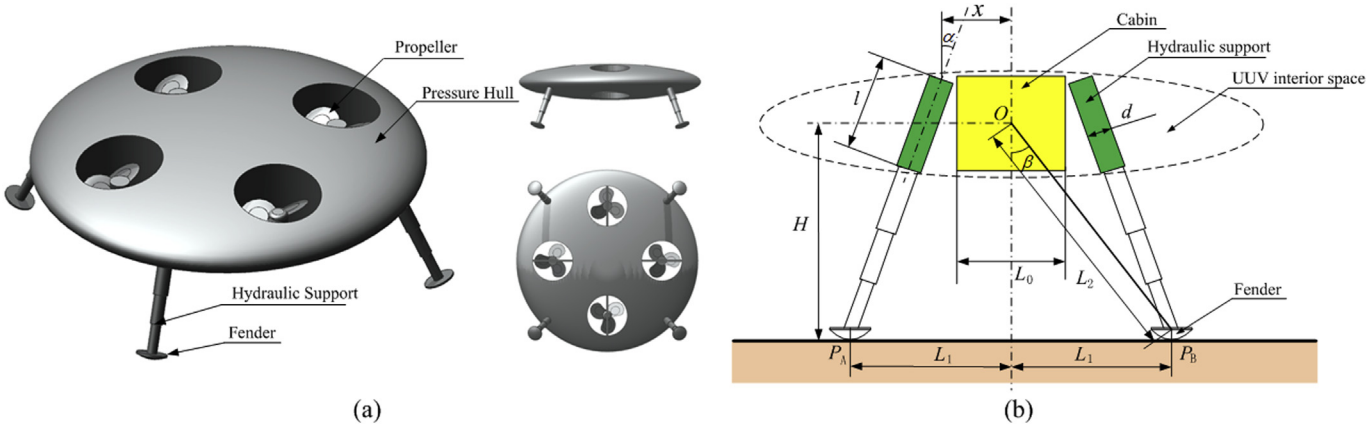

Fig. 2. (a) an external view and Fig. 2(b) an internal structure view of landing platform.

Table 1
Parameters of landing platform.

Parameters	Explanation	Value	Parameters	Explanation	Value
The FRDS UUV parameters					
L_D/mm	Long axis of elliptical	1000	L_0/mm	Length of cabin	200
L_d/mm	Short axis of elliptical	200	H/mm	Height of buoyancy center	–
G/N	Gravity	845	L_1/mm	Distance from the central axis	–
N/N	Buoyancy	825	L_2/mm	Length of force arm	–
Hydraulic support parameters					
Num.	Number of stages	3	x/mm	Distance from the center	–
d_H/mm	Hydraulic support diameter	45	α/deg.	Inclination angle	–
d_F/mm	Fender diameter	60	l /mm	Length of hydraulic support	–

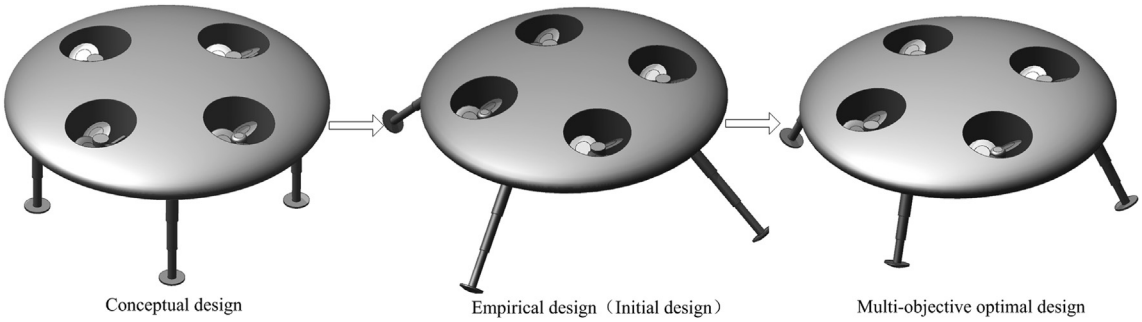

Fig. 3. The optimization procedure.

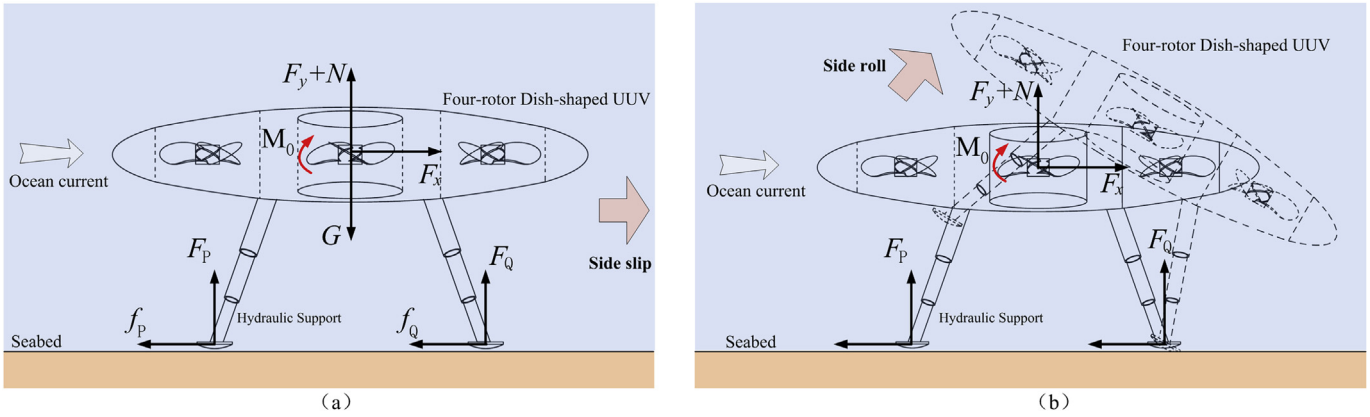

Fig. 4. Two kinds of instability type: (a) Side slip and (b) Side roll.

The second kind of instability type: Side roll. When the fluid torque of the FRDS UUV and the hydraulic support relatively to the rear fulcrum P_B exceeds the restoring torque from residual gravity ΔG, side roll occurs. Meanwhile, the support force F_P of the front fulcrum P_A tends to zero. The mathematical model for the critical state can be obtained:

$$\lim_{F_P \to 0} F_P \cdot 2L_1 + F_x \cos\beta \cdot L_0 + M_L + F_y \cdot L_1 - \Delta G \cdot L_1 \geq 0 \tag{3}$$

$$\Delta G = G - N \tag{4}$$

$$\beta = \arctan\frac{L_1}{H} \tag{5}$$

where M_L is the hydrodynamic torque of the hydraulic support; L_0 is the length of force arm; ΔG represents residual gravity; β is the inclined angle.

After the optimization design, the hydrodynamic characteristics of landing platform can be obtained. According to the mathematical model Eqs. (1) and (3) for the critical state, we could determine the landing attitude, and whether or not to adjust UUV parameters such as residual gravity ΔG to maintain the stable attitude. The main goal of the paper is to optimize the design of the appearance and layout design for hydraulic support system, so the internal control details are not described here. In order to obtain the optimal hydrodynamic performance, 5 sub optimization objectives are proposed. The optimization procedure is described in detail in the following sections.

3. Numerical method

3.1. Governing equations

The governing equations for the landing platform are the Reynold-Averaged Navier Stokes (RANS) equations for incompressible viscous flow (Sun et al., 2015). The RANS equations including the continuity equation and momentum equation are given below:

$$\nabla \cdot U = 0 \tag{6}$$

$$\rho\overline{u}_j\frac{\partial\overline{u}_i}{\partial x_j} = \rho\overline{f}_i + \frac{\partial}{\partial x_j}\left[-\overline{p}\delta_{ij} + \mu\left(\frac{\partial\overline{u}_i}{\partial x_j} + \frac{\partial\overline{u}_j}{\partial x_i}\right) - \rho\overline{u_i'u_j'}\right] \tag{7}$$

whereρ is the density of fluid; U is the relative velocity; μ is liquid viscousness; δ_{ij} is Kronecker delta; $\overline{f}_i$ is mass force term; $-\rho\overline{u_i'u_j'}$ is apparent stress owing to the fluctuating velocity field, generally referred to as the Reynolds stress.

The turbulence model is required to adapt to a wide range, so SST k−ω model is selected for the hydrodynamic numerical simulation in this paper.

Turbulence intensity equation

$$\frac{\partial\rho k}{\partial t} + \nabla(\rho k U) = \nabla\left[\left(\mu + \frac{\mu_z}{\sigma_k}\right)\nabla k\right] + p_k - b_k\rho k\omega \tag{8}$$

Turbulent frequency equation

$$\frac{\partial\rho\omega}{\partial t} + \nabla(\rho\omega U) = \nabla\left[\left(\mu + \frac{\mu_z}{\sigma_\omega}\right)\nabla\omega\right] + a\frac{\omega}{k}p_k - b_\omega\rho k\omega^2 \tag{9}$$

where p_k is kinetic energy; σ_k and σ_ω are turbulent Prandtl numbers; $\mu_z = \rho k/\omega$ represents eddy viscosity.

3.2. Computational domain and grid generation

Ansys CFX is used to simulate the interaction of liquids with surfaces defined by boundary conditions for the landing platform. The boundaries of the flow field are built. The external flow field is transformed into the internal flow problem with reference to the research. The computational domain and mesh size have been determined through the analysis of grid independence and boundary effects for the following simulation. The shape of computational domain is shown in Fig. 5, and the boundary conditions are set as follows:

1) Inlet: The inlet velocity at the front of the fluid domain was set to be equivalent to the UUV velocity, 1 m/s.
2) Outlet: The pressure on the outlet of the domain was set to be 0 Pa.
3) Free slip wall: Free wall conditions were set at the top, left and right side walls.

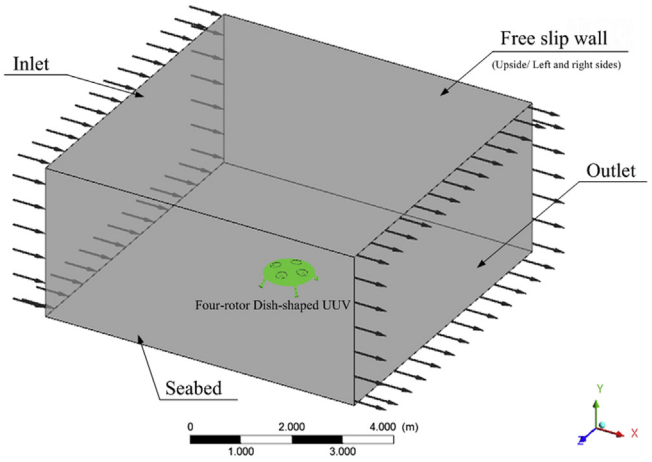

Fig. 5. Computational domain.

4) No slip wall: No slip wall conditions were set at the bottom wall (the seabed) and the surfaces of the UUV and the hydraulic supports.

The FRDS UUV landing platform has a complicated shape and 4 perforating passages. In order to ensure the accuracy of the calculation, the propellers are retained in the CFD numerical simulation. 1.8 million unstructured grids are defined after the grid independence test. The unstructured grids can keep the angle and area effectively for curved surfaces. Tetrahedral grids are used in the calculations presented here. As shown in Fig. 6(a), the grid density is higher around the landing platform to precisely describe the profiles of the platform. Fig. 6(b) shows the grid structure on the surfaces of the UUV.

Grid independence test was carried by compared the drag F_x and lift F_y of landing platform changing with α. Two different grid densities were studied. Data1 was obtained by about 1.8 million unstructured grids, while data1 was obtained by about 4.5 million unstructured grids. Two kinds of simulation dates have great consistency with reference data obtained by experience, as shown in Fig. 7.

The pressure distribution on the surfaces of UUV was shown in Fig. 8. There is a significant high pressure zone at the fronts of the UUV and hydraulic supports. The overall pressure is lower at four propeller areas due to the reverse flow. Separation flow occurs at the back of the landing platform. Pressure distribution is not uniform at the surfaces of the landing platform, which provides the external force and torque of landing platform from flow field.

4. Multi-objective programming

Multi-objective Programming (MOP) of the hydraulic support landing platform was proposed. 5 sub objectives were proposed to get the optimal comprehensive performances. Sub objective functions were established respectively, such as minimal torque ($Min\ M_z(\mathbf{X})$), minimal lift ($Min\ F_y(\mathbf{X})$), minimal drag ($Min\ F_x(\mathbf{X})$), maximal height ($Max\ H(\mathbf{X})$) and minimal volume ($Min\ V(\mathbf{X})$). According to the actual demand, the constraint conditions were derived from the geometric relation, as shown in Eq. (10). So the multi-objective function of the whole landing platform system could be defined:

$$\mathbf{X} = (x, \alpha)^T$$

$$\left[Min\, M_z(\mathbf{X}),\ Min\, F_y(\mathbf{X}),\ Min\, F_x(\mathbf{X}),\ Max\, H(\mathbf{X}),\ Min\, V(\mathbf{X})\right]^T$$

$$s.t.:\ 200 \le x \le 500$$

$$0 \le \alpha \le \arctan\left(\frac{500 - x}{\sqrt{(1 - x^2/D^2)d^2}}\right) \tag{10}$$

Firstly, 5 sub objective functions have different units. Dimensionless method is applied for the objective function. Dimensionless method is carried out as follows:

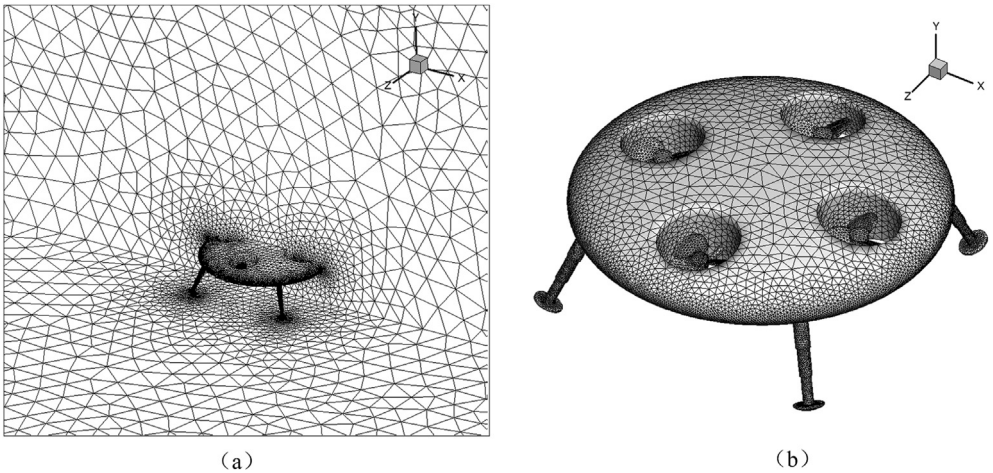

(a) (b)

Fig. 6. (a) Grid structure around the landing platform (b) Grid structure in the FRDS UUV's surfaces.

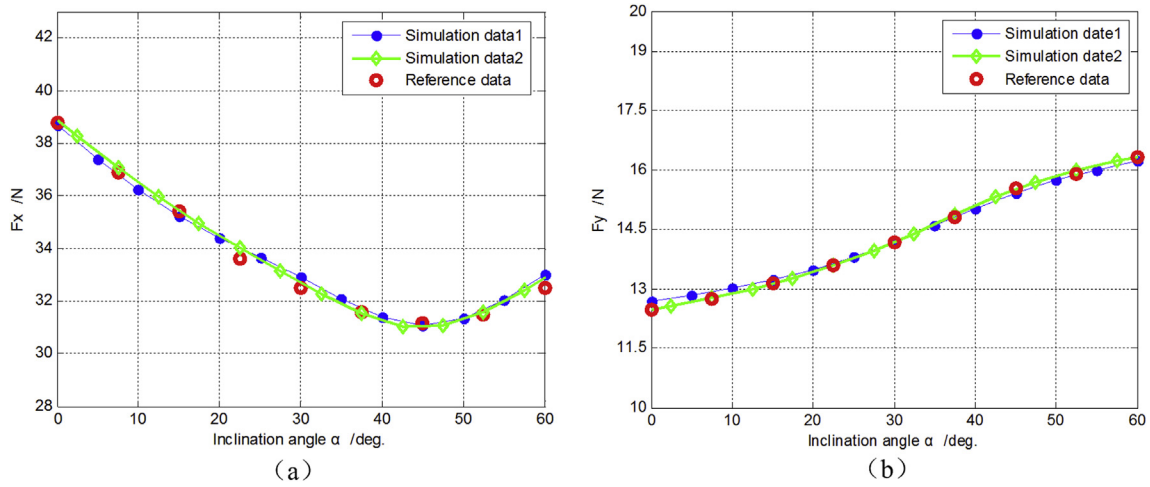

Fig. 7. Grid independence test: (a) drag (b) lift.

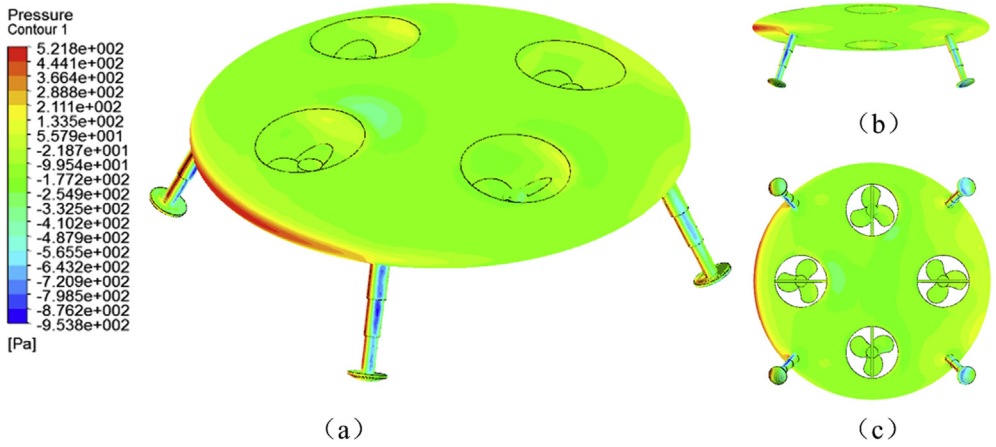

Fig. 8. The pressure distribution on the surfaces of the FRDS UUV.

$$f_i^{(1)}(X) = \frac{f_i^{(0)}(\mathbf{X})}{average\left(f_i^{(0)}(\mathbf{X})\right)} \quad i = 1,2,3,4,5 \tag{11}$$

$f_i^{(0)}(\mathbf{X})$ is the i th sub objective function;
$f_i^{(1)}(\mathbf{X})$ is the i th sub objective function after dimensionless method.

Then, there are different optimization directions for the sub objective functions. *Min* $M_z(\mathbf{X})$, *Min* $F_y(\mathbf{X})$, *Min* $F_x(\mathbf{X})$ and *Min* $V(\mathbf{X})$ are minimal optimization problems, while *Max* $H(\mathbf{X})$ is maximal optimization problem. Unification of optimization direction for 5 sub objective functions should be considered. Considering the consistency and convenience of PSO algorithm, *Min* $M_z(\mathbf{X})$, *Min* $F_y(\mathbf{X})$, *Min* $F_x(\mathbf{X})$ and *Min* $V(\mathbf{X})$ are converted into maximization optimization problems as follows:

$$f_i(\mathbf{X}) = \frac{1}{f_i^{(1)}(\mathbf{X})} \quad i = 1,2,3,5 \tag{12}$$

Max $H(\mathbf{X})$ is maximal optimization problem, so no conversion is necessary for $f_4^{(1)}(\mathbf{X})$.

Finally, according to the important degree of each sub objective, corresponding weight ω_i was defined by important degree. 5 weights of sub objectives were given according to the experience of engineering in advance, so "Multi-objective optimization" can be translated into solvable "Single Objective Optimization (SOP)". The transformation is just a solving method, which makes it more efficient to obtain optimal solution. 5 sub objective functions are added to build a global objective function $MOF(\mathbf{X})$.The optimization model Eq. (10) is further transformed into:

$$\begin{aligned} &\mathbf{X} = (x,\alpha)^T \\ &MOF(\mathbf{X}) = Max\left[\sum_{i=1,2,3,5}^{4} \omega_i \cdot f_i(\mathbf{X}) + \omega_4 \cdot f_4^{(1)}(\mathbf{X}),\right] \\ &s.t.:\ 200 \le x \le 500 \\ &0 \le \alpha \le \arctan\left(\frac{500 - x}{\sqrt{(1 - x^2/D^2)d^2}}\right) \end{aligned} \tag{13}$$

The weights satisfy the normalization and non-negative condition:

$$\sum_{i=1}^{5}\omega_i = 1 \quad \omega_i \geq 0 \tag{14}$$

According to the actual engineering experience, the weights of $\omega_i i = 1,2,3,4,5$ was defined to determine the important degree of an objective. The weights were prepared from expert evaluating. For better understanding, the sub objective functions at different stages and weighs are listed in Table 2.

5. Response surface model

The response surface model is a mathematical method to obtain the model of objective function based on the theory of Design of Experiment (DOE). DOE is the base of approximate model. DOE is the design of a task that aims to predict the variation of information under conditions that are hypothesized to reflect the variation. DOE involves not only the selection of suitable predictors and outcomes, but planning the delivery of the experiment under statistically optimal conditions given the constraints of available resources. So the number of sample points should be sufficient that these points can be spread over the design space uniformly (Sun et al., 2015). 30 initial samples (design schemes) were identified and resolved by orthogonal design for the response surface model. The hydrodynamic characteristics of 30 samples were evaluated by Ansys CFX.

Polynomial response surface is a frequently used approximation method in engineering. The mathematical expression is shown as follows:

$$f(\mathbf{X}) = \beta_0 + \sum_{i=1}^{m}\beta_i + \sum_{i=1}^{m}\sum_{j=1}^{m}\beta_{ij}\cdot x_i x_j + \ldots \tag{15}$$

where x_i is ith component of m-dimension argument; β_0, β_i and β_{ij} constitute a vector $\boldsymbol{\beta}$ by arranged in a certain order. The key to solving the polynomial approximate model is to get the vector $\boldsymbol{\beta}$. The construction of response surface is the process of the regression analysis of the samples. The least square method has the ability to smooth the numerical fluctuation. It is widely used in the regression analysis. In order to solve easily, Eq. (15) is further transformed into:

$$f\left(x^k\right) = \mathbf{X}^k\boldsymbol{\beta} \quad k = 1,2,3\cdots n \tag{16}$$

where $\mathbf{X}^k$ is the kth line vector which consists of variables; the dimension of $\boldsymbol{\beta}$ is$(m + 2)(m + 1)/2$.

In this paper, X^1 and X^2 represent x and α, respectively. $\mathbf{X}^k = (x^k,\alpha^k)$ is established. So Eq. (16) can be replaced by:

$$f\left(\mathbf{X}^k\right) = f\left(x^k,\alpha^k\right) = Y^k \tag{17}$$

Therefore, polynomial equation is generalized obtained.

$$\mathbf{X}\cdot\beta = \mathbf{Y} \tag{18}$$

where $\mathbf{X} = [X^1,X^2,\ldots,X^k,\ldots,X^n]^T$ represents the variables of sample point; $\mathbf{Y} = [Y^1,Y^2,\ldots,Y^k,\ldots,Y^n]^T$ represents corresponding value. Generally, n is greater than $(m + 2)(m + 1)/2$ and the rank of $\mathbf{X}$ is less than n, so $\mathbf{X}^T\mathbf{X}$ is non-singular. Therefore, $\widehat{\boldsymbol{\beta}}$ can be obtained:

$$\widehat{\boldsymbol{\beta}} = \left[\mathbf{X}^T\mathbf{X}\right]^{-1}\mathbf{X}^T\mathbf{Y} \tag{19}$$

Response surface model $f(\mathbf{X})$ is updated by.

$$\widehat{f}(\mathbf{X}) = \mathbf{X}\cdot\widehat{\boldsymbol{\beta}} = f(\mathbf{X}) - \delta \tag{20}$$

The regression error of least squares estimation δ can be defined as follows:

$$\delta^2 = \sum_{i=1}^{30}|f(x_i) - y_i|^2 \tag{21}$$

Meanwhile, the value $\mathbf{Y}(f_1(\mathbf{X}))$ of sub objective functions can be obtained after being translated from $Min\ M_z(\mathbf{X})$ in Eqs. (10)–(13), as shown in Table 3.

The high order fitting model of $f_1(\mathbf{X})$ is constructed based on these samples. 30 samples and response surface are shown in Fig. 9.

Similarly, high order response surface models of other 4 sub objectives are obtained, as shown in Fig. 10. Fig. 10(a) shows the response surface of $f_2(\mathbf{X})(Min\ F_y(\mathbf{X}))$. Fig. 10(b) shows the response surface of $f_3(\mathbf{X})$ $(Min\ F_x(\mathbf{X}))$. Fig. 10(c) shows the response surface of $f_4(\mathbf{X})(Max\ H(\mathbf{X}))$. Fig. 10(d) shows the response surface of $f_5(\mathbf{X})(Min\ V(\mathbf{X}))$.

The response surface model of the global objective function $MOF(\mathbf{X})$ is built in the next section with optimization result, as shown in Fig. 12.

Table 3
Objective value $\mathbf{Y}(f_1(\mathbf{X}))$after dimensionless method and unified optimization directions.

Objective value **Y** after conversion		Inclination angle α/deg.				
		0	15	30	45	60
Distance from the center x/mm	200	0.7242	0.7553	0.7859	0.8365	0.9368
	260	0.7784	0.8360	0.8635	0.9482	1.0932
	320	0.9252	0.9808	1.0903	1.1665	1.1466
	380	1.2210	1.2869	1.3377	1.2569	1.1134
	415	1.5525	1.4534	1.3877	1.2476	0.8980
	440	1.2984	1.1282	0.8741	0.8119	0.7317

Table 2
Objective functions and weights.

Objective function	5 sub objective functions				
	$Min\ M_z(\mathbf{X})$	$Min\ F_y(\mathbf{X})$	$Min\ F_x(\mathbf{X})$	$Max\ H(\mathbf{X})$	$Min\ V(\mathbf{X})$
Initial status	$f_1^{(0)}(\mathbf{X})$	$f_2^{(0)}(\mathbf{X})$	$f_3^{(0)}(\mathbf{X})$	$f_4^{(0)}(\mathbf{X})$	$f_5^{(0)}(\mathbf{X})$
Dimensionless method	$f_1^{(1)}(\mathbf{X})$	$f_2^{(1)}(\mathbf{X})$	$f_3^{(1)}(\mathbf{X})$	$f_4^{(1)}(\mathbf{X})$	$f_5^{(1)}(\mathbf{X})$
Unified optimization directions	$f_1(\mathbf{X})$	$f_2(\mathbf{X})$	$f_3(\mathbf{X})$	$f_4^{(1)}(\mathbf{X})$	$f_5(\mathbf{X})$
Weights	$\omega_1 = 0.3$	$\omega_2 = 0.25$	$\omega_3 = 0.2$	$\omega_4 = 0.1$	$\omega_5 = 0.05$

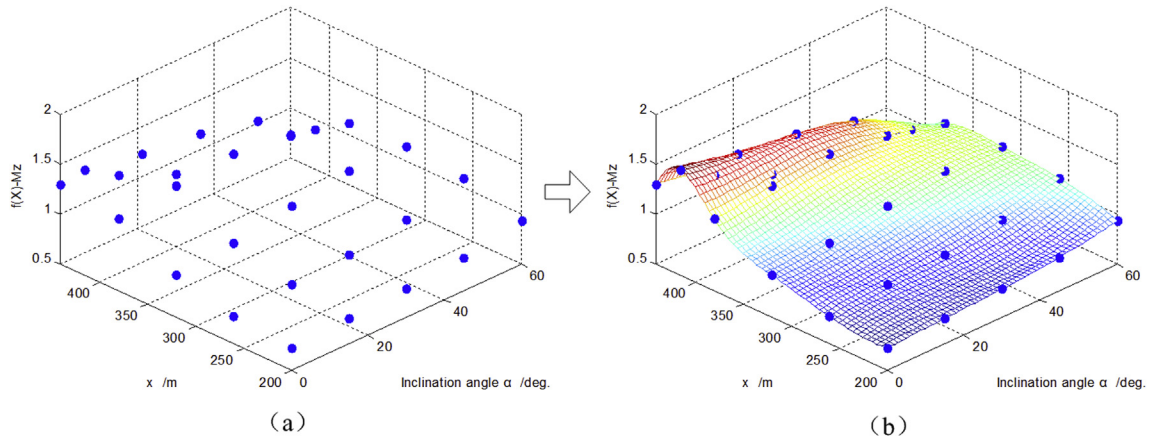

Fig. 9. Establish process of response surface model of $f_1(\mathbf{X})$.

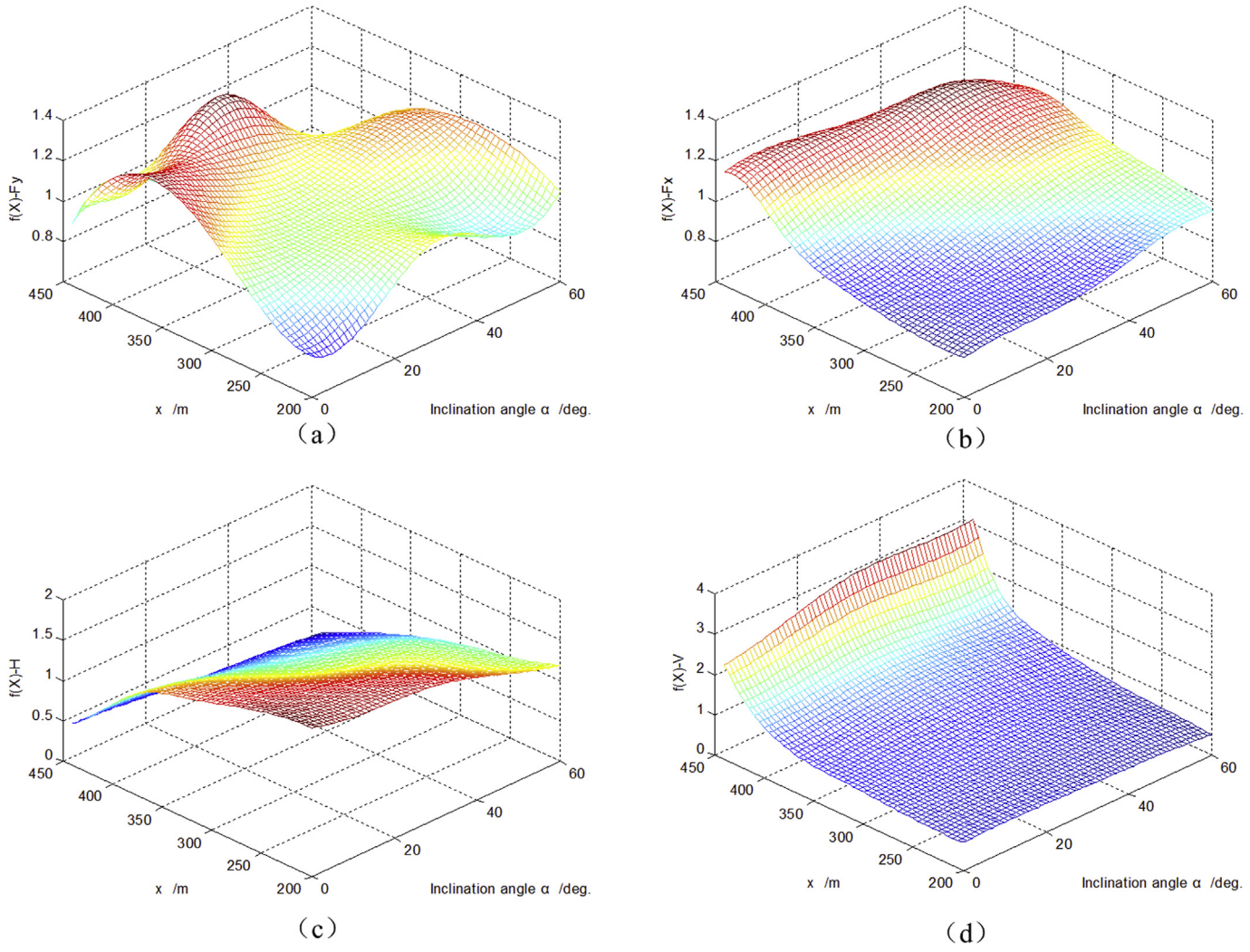

Fig. 10. Response surface of 4 sub optimization objectives.

6. Particle swarm optimization

A Particle Swarm Optimization (PSO) algorithm was applied in the multi-objective design of the hydraulic support landing platform. PSO is an evolutionary computation technique (Kennedy and Eberhart, 1995). PSO algorithm simulates bird collective behavior. Using the information from individual in the group, the movement of the whole group is generated from disorder to order in the problem solving space, and the optimum solution is obtained.

During optimization process, PSO was compared with Genetic Algorithm (GA) which is also global optimization methods. In this paper, 1000 particles were randomly selected in PSO. After about 500–600 iterations, optimal solution was obtained. And in the similar case, GA-based iteration takes up to 2–3 times as long as PSO-based iteration for this optimization. So PSO was identified. More specifically, PSO has the advantages of: it has a simple concept and can be implemented on a computer; the optimization problem has low requirements including a black box, without requiring the explicit expression; it has quicker convergence speed and optimal solutions can be obtained in acceptable computation cost; it has the strong ability in global search which will avoid trapping in local optimum (Chen et al., 2008). The steps of PSO are given:

1) Initialize particle.
2) Calculate the fitness value.
3) Choose the particle with the best fitness value of all the particles as the optimal solution.
4) If the fitness value is satisfied in history, set the optimal solution as the global optimal solution.
5) Otherwise, calculate particle speed and fitness value, and update particle position.
6) Calculate the optimal solution of particle swarm.
7) Determine whether fitness value is satisfied and carry out the next step 'Loop or End'.

Fig. 11 shows the detailed general procedure of PSO:

The given procedure has been implemented here in a computer program (using Matlab language) to solve the optimization problem and make it automatic.

Finally, according to response surface of the objective function *MOF*(**X**), optimal position is numerically solved as shown in Fig. 12. The optimal point and initial point are marked in Fig. 12. The optimal solution illustrates the effectiveness and validity of the proposed algorithm.

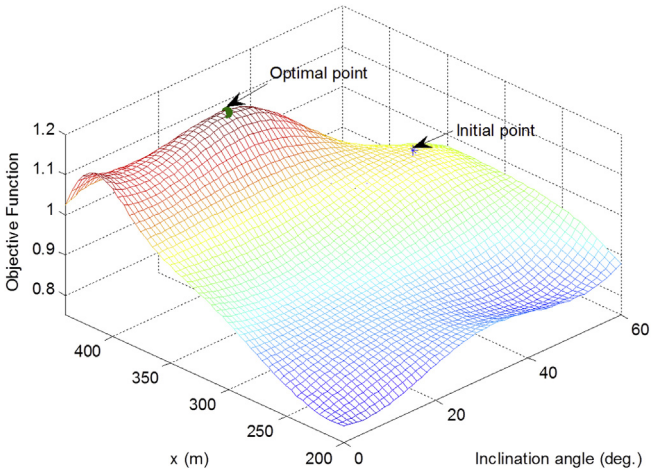

Fig. 12. Response surface of the global objective function *MOF*(**X**) and with optimization result.

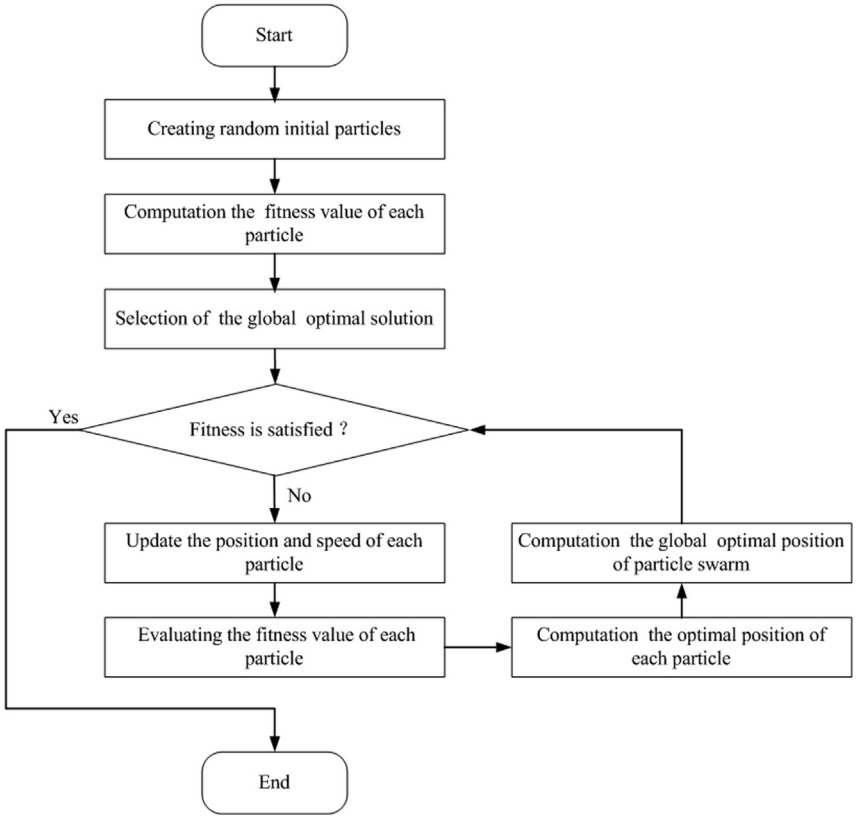

Fig. 11. The general procedure of PSO.

Table 4
Main design parameters of landing platform.

Design parameters	Optimal design	Initial design
x/mm	406.97	320
α/deg.	26.52	45
l/mm	75	125
L_1/mm	548.89	680
L_2/mm	599.18	750

Through the iterative search for the optimal solution, the identification parameters were directly obtained by PSO. Main design parameters of landing platform are compared in Table 4.

Table 5
Optimization results: values of optimization objectives of landing platform.

	Optimal design	Initial design	Weight	Optimization effect
Torque M_Z/N m	−12.9372	−15.4885	0.3	+16.47%
Lift F_y/N	13.6883	16.4917	0.25	+16.97%
Drag F_X/N	32.2349	34.5835	0.2	+6.79%
Height H/m	0.2702	0.3038	0.1	−11.03%
Volume V/dm^3	1.3927	1.9179	0.05	+27.38%
Global objective index	1.158	1.045	1	+10.86%

7. Results and discussion

After optimization, sub objectives and global objective can be obtained. Torque M_Z, lift F_y, drag F_x and volume V are improved. But height H becomes lower. As for MOP, some smaller weight objectives may not be optimized. Initial values and optimal values are compared, as shown in Table 5.

The different coupling constraints and the sensitivity to variables may result in an opposite direction for optimization problems. Once the global objective is optimized, the optimization results can be accepted. We can confirm that the global objective index changes from 1.045 to 1.158. This result shows that the optimization process successfully improved the initial design. So the global optimum design is obtained. The results show that the optimization process has the better performance.

Figs. 13 and 14 show streamlines and pressure distribution around the optimal design and initial design separately. They have a similar pressure distribution. But the distance between the FRDS UUV and the seabed is shorter compared with initial design. Wall effect becomes more obvious. The velocity of the flow is bigger and the pressure is lower. It will press down on the landing platform into the seabed eventually.

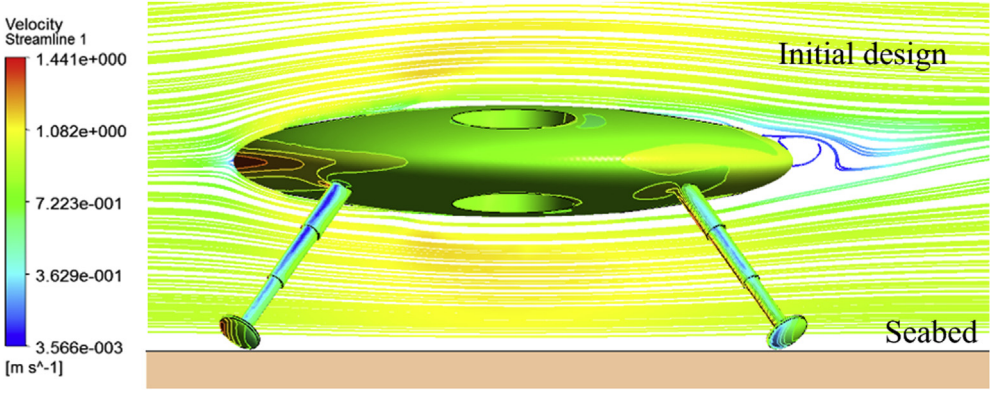

(a)

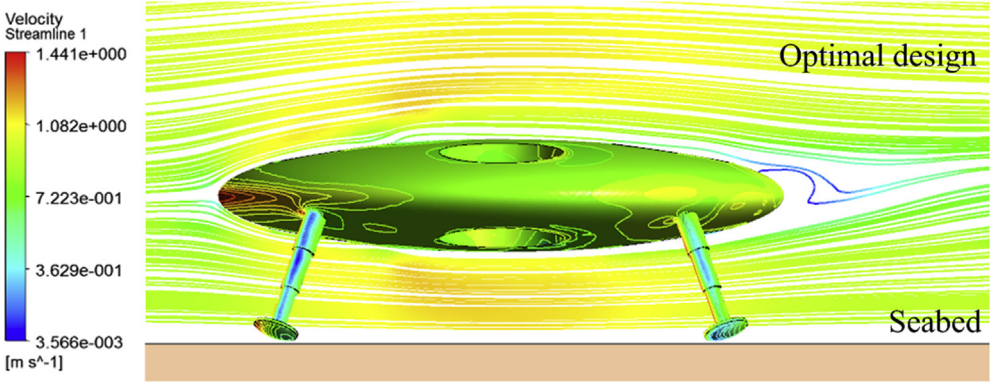

(b)

Fig. 13. Side view: stream lines and pressure distribution.

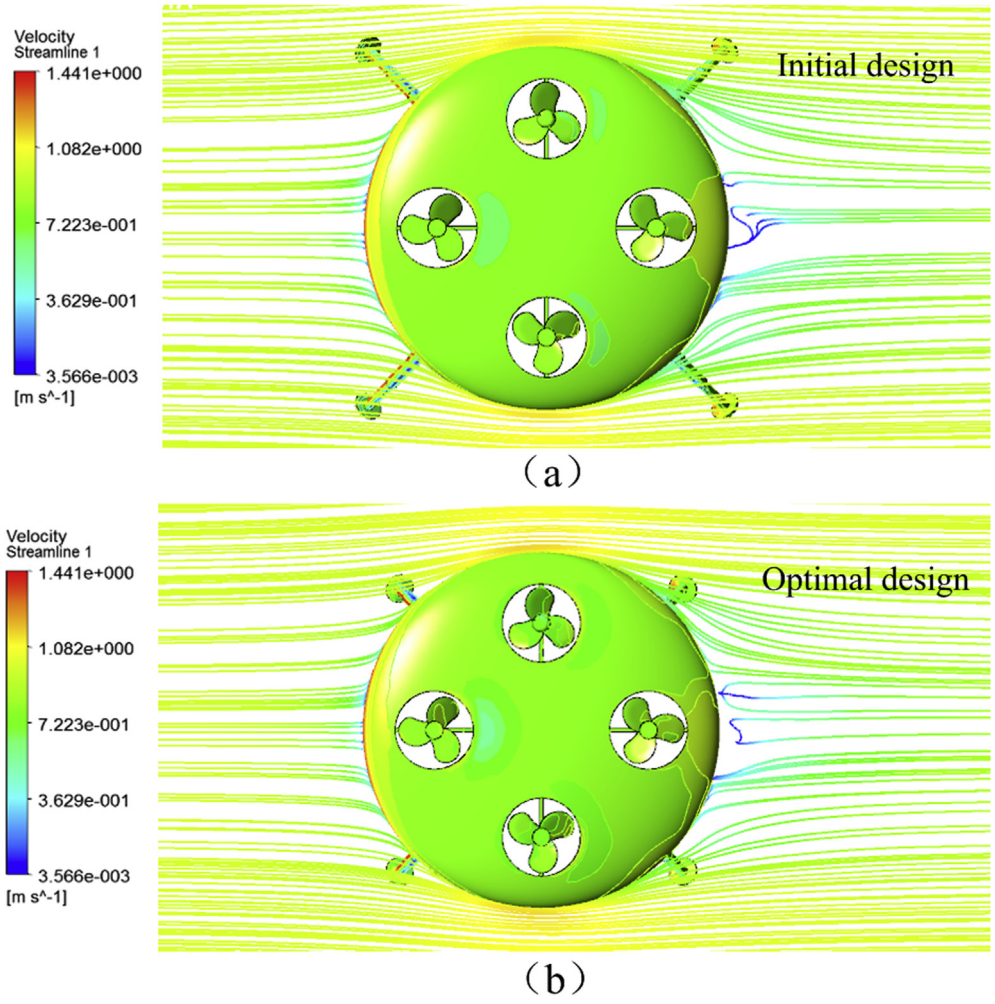

Fig. 14. Plan view stream lines and pressure distribution.

8. Conclusions

A PSO algorithm was presented to obtain the optimal design of hydraulic support landing platform. The hydrodynamic characteristics of the landing platform were evaluated using Ansys CFX. Based on 30 sample points (design schemes), high order response surface models were established accurately. PSO was precisely used to found optimal design. By summarizing the optimization result of this study, we conclude as follows:

(1) The global objective index of the landing platform is obviously better than initial design (empirical design). The global objective index has been enhanced by 10.86% (from 1.045 to 1.158).
(2) Apparently, Torque M_Z, lift F_Y and volume V of landing platform are improved, while the height H with a smaller weight is not improved. The optimization efficiency becomes degraded gradually when solving a large numbers of sub objectives. So individual goal may not be optimized simultaneously, which is inevitable in general.
(3) Volume V has high sensitivity to be optimized, but contributions of V are smaller. Greater contributions correspond to higher weights. Other sub objectives such as Torque M_Z and lift F_Y have higher weights, which should be valued highly to improve the whole performances.

In this paper, the FRDS UUV has been designed and manufactured. The optimization result of landing platform for the FRDS UUV will be taken into account in the future. These analysis and optimization results provide a theoretical guidance and reference. Further research and experiment are directed to the experience of the landing platform investigating the influence of the ocean environmental factors.

Acknowledgment

The authors would like to acknowledge the support of the Grant No.51179159 from the National Natural Science Foundation of China.

References

Agrawal, R.K., Bawane, N.G., 2015. Multi-objective PSO based adaption of neural network topology for pixel classification in satellite imagery. Appl. Soft Comput. J. 28, 217–225.

Andrews, P.S., 2006. An investigation into mutation operators for particle swarm optimization. IEEE Congr. Evol. Comput. 1044–1051.

Angeline, P.J., 1998. Using selection to improve particle swarm optimization. IEEE Int. Conf. Comput. 84–89.

Cerveira, Frederico, Fonseca, Nuno, Pascoal, Ricardo, 2013. Mooring system influence on the efficiency of wave energy converters. Int. J. Mar. Energy 3–4, 65–81.

Chan, K., Dillon, T.S., Chang, E., 2013. An intelligent particle swarm optimization for short-term traffic flow forecasting using on-road sensor systems. IEEE Trans. Ind. Electron 60, 4714–4725.

Chen, P., 2015. Two-level hierarchical approach to unit commitment using expert system and elite PSO. IEEE Trans. Power Syst. 27, 780–789.

Chen, H.N., Zhu, Y.L., Hu, K.Y., Ku, T., 2008. Global optimization based on hierarchical convolutions model. IEEE Congr. Evol. Comput. 1497–1504.

Eberhart, R., Kennedy, J., 1995. A New Optimizer Using Particle Swarm Theory. International Symposium on MICRO Machine and Human Science, Nagoya, Japan, pp. 39–43.

Feng, Z., Allen, R., 2004. Evaluation of the effects of the communication cable on the dynamics of an underwater flight vehicle. Ocean Eng. 31, 1019–1035.

Hu, Fengjun, Wu, Fan, 2010. Diploid hybrid particle swarm optimization with differential evolution for open vehicle routing problem. Eighth World Congr. Automatic Control Artif. Intell. 20, 2692–2697.

Huston, R.L., Kamman, J.W., 1982. Validation of finite segment cable models. Comput. Struct. 15 (6), 653–660.

Jin, N., Rahmat-Samii, Y., 2010. Hybrid real-binary particle swarm optimization (HPSO) in engineering electromagnetics. IEEE Trans. Ant. Prop. 58, 3786–3794.

Juang, C.F., 2004. A hybrid of genetic algorithm and particle swarm optimization for recurrent network design. IEEE Trans. Syst. Man Cybern. B Cybern 34, 997–1006.

Kennedy, J., Eberhart, R., 1995. Particle Swarm Optimization, vol. 4. IEEE International Conference on Neural Networks, Piscataway, NJ, pp. 1942–1948.

Liang, J.J., Qu, B.Y., Suganthan, P.N., et al., 2012. Dynamic multi-swarm particle swarm optimization for multi-objective optimization problems. IEEE Congr. Evol. Comput. 22 (10), 1–8.

Sun, Chunya, Song, Baowei, Wang, Peng, 2015. Parametric geometric model and shape optimization of an underwater glider with blended-wing-body. Int. J. Nav. Archit. Ocean Eng. 7, 995–1006.

Song, Baowei, Zhu, Xinyao, San, Zhixiong, et al., 2012. Hydrodynamic characteristics and stability analysis of UUV (Unmanned Underwater Vehicle) parking on the seabed. J. Northwest. Polytech. Univ. 30 (1), 94–101.

Song, Bao-wei, Zhang, Bao-shou, Jiang, Jun, et al., 2016. Estimation of equation of motion of four-rotor dish-shaped AUV and simulation research on its hydrodynamic characteristics. Acta Armamentarii 37 (2), 299–306.

Wang, Li-Zhong, Guo, Zhen, Yuan, Feng, 2010. Three-dimensional interaction between anchor line and seabed. Appl. Ocean Res. 32, 404–413.